Nanoscale

Accepted Manuscript

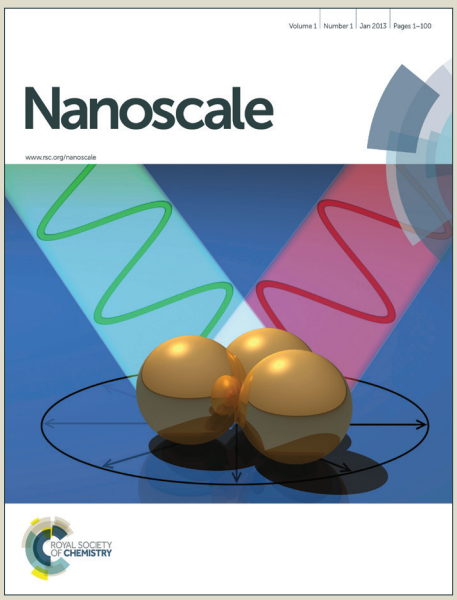

ROYAL SOCIETY OF CHEMISTRY

www.rsc.org/nanoscale

Table of contents entry

A composite with $FeCl_2$ nanocrystals sandwiched between Cl-doped graphite layers was created as a new type of anode material for Li-ion batteries exhibiting high performance.

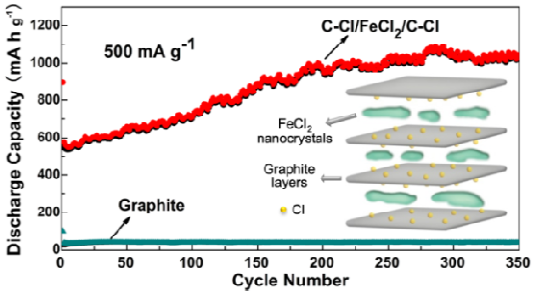

Cite this: DOI: 10.1039/c0xx00000x

www.rsc.org/xxxxxx

COMMUNICATION

$FeCl_2$-graphite sandwich composite with Cl doping in graphite layers: A new anode material for high-Performance Li-Ion batteries

Lili Wang, Cong Guo, Yongchun Zhu,* Jianbin Zhou, Long Fan and Yitai Qian*

Received (in XXX, XXX) Xth XXXXXXXXX 20XX, Accepted Xth XXXXXXXXX 20XX

DOI: 10.1039/b000000x

A composite with $FeCl_2$ nanocrystals sandwiched between Cl-doped graphite layers has been created via a space-confined nanoreactor strategy. This composite can be used as a new type of anode material for Li-ion batteries, which exhibit high reversible capacity and superior rate capability with excellent cycle life.

Rechargeable Li-ion batteries (LIBs) are one of the most important power sources for portable electronic devices, electric vehicles and energy storage systems.[1] However, the existing anode materials, such as graphite, have a limited specific capacity, representing a great challenge to meet the fast increasing demand for high-power rechargeable LIBs. The use of carbonaceous nanocomposites has been regarded as one of the most promising approaches to achieve higher energy density and better rate capability.[2] Success has been made to improve the specific capacity and cyclability significantly through sandwiching chemically stabled anode materials between carbon layers. Examples are the smartly designed sandwich-like graphene-based titania nanosheets,[3] graphene-SnO_2 sandwich structure,[4] Fe_2O_3 sandwiched in graphene,[5] Sn-graphene sandwich structure,[6] TiO_2/graphene sandwich paper,[7] and so on.[8-10] To explore new possibilities for anodes, it is desirable to design the sandwich-structured carbon composite to achieve the application of unstable materials in LIBs.

Another common and promising strategy to enhance the electrochemical performance of carbonaceous anodes is doping. Compared to pure carbon structures, an enhanced specific capacity has been demonstrated through doping carbon materials, most including adsorption and doping of phosphorus,[10] boron,[12,13] and nitrogen.[5,12,14-16] However, carbon with Cl-doping has not been explored as electrode materials yet, although previous report has shown that the p-doping of graphite with chlorine could improve its conductivity.[17,18] Moreover, a conjugated system may form between carbon and chlorine after doping, since the π-electrons transfers from graphite to chlorine.[19-21] Such interesting features of Cl-doping inspires us to study whether Cl-doping is favorable to enhance the electrochemical performance of LIBs or not.

Here we combine both approaches and synthesize a composite with $FeCl_2$ nanocrystals sandwiched between Cl-doped graphite layers (C-Cl/$FeCl_2$/C-Cl) as a new type of anode material for LIBs. It was prepared from the stage 2 $FeCl_3$-graphite intercalation compounds ($FeCl_3$-GICs) through the thermal decomposition $FeCl_3 \rightarrow FeCl_2$+ Cl within the graphite interlayers, as schematically illustrated in Figure S1. In this approach, the graphite layers act as a space-confined nanoreactor, which can avoid the fast aggregation of $FeCl_2$ nanocrystals, and also can suppress the release of Cl and trap Cl to form C-Cl and an intercalation of Cl in graphite layers, exhibiting π-electron delocalization effect, which is favorable to increasing the electric conductivity and could be benefit to the storage of Li-ions. Besides, this sandwich structure has effectively inhibited the instability of $FeCl_2$ nanocrystals in environment due to the protection of impermeable graphite layers. As an anode material, the C-Cl/$FeCl_2$/C-Cl delivers a high reversible capacity and a superior rate capability with excellent cycle life, which could be attributed to the combinative merits of $FeCl_2$ nanocrystals, sandwiched structures and Cl-doping of graphite layers with π-electron delocalization effect.

Figure 1a, b present the XRD patterns of the as-prepared composite and the stage 2 $FeCl_3$-GICs which was synthesized as we previously reported.[22] All the peaks in Figure 1a can be indexed to rhombohedral-phase $FeCl_2$ (JCPDS Card, No 70-1634) and Hexagonal-phase graphite (JCPDS Card, No 25-0284). Compared with the peaks in Figure 1b of the stage 2 $FeCl_3$-GICs, it is notable that the graphite in as-prepared product does not display any staging effect, indicating the product is no longer a graphite intercalation compound, but a composite of $FeCl_2$ and graphite. The average crystallite size of the $FeCl_2$ is about 28 nm calculated using the Scherrer equation. The $FeCl_2$ content of the as-prepared sample determined by X-ray fluorescence spectroscopy (XRF) is approximately 34.3 wt%.

The morphology and microstructure of the C-Cl/$FeCl_2$/C-Cl are characterized by transmission electron microscopy (TEM) and field-emission scanning electron microscopy (FESEM). As shown in **Figure 2**a, the C-Cl/$FeCl_2$/C-Cl exhibites sheet structure which inherits the morphology and size of EG with two-dimensional scale of several tens of micrometers (see Figure S2 for Low-magnification and high-magnification SEM images). From TEM image, there is a notable contrast difference in the composite, showing pale sheets and the dark inlays, and similar phenomenon can be observed from SEM image (Figure S2). The high-resolution TEM (HRTEM) images of the C-Cl/$FeCl_2$/C-Cl provide evidence of the sandwich structure. Figure 2b clearly present the (002) fringes of graphite with lattice fringe spacing of about 3.45 Å. Among the lattice fringe of graphite, other two distinguishable fringes can be observed as highlighted by dotted

box in Figure 2b. From the magnified images of the fringes (Figure 2c and 2d), the d-spacing values of the lattice planes are 1.72 and 2.54 Å, which correspond well with those of (113) and (104) planes of the Rhombohedral $FeCl_2$ crystals, respectively. Energy-dispersive x-ray (EDX) mapping analysis was conducted to further investigate the element distribution in the composite. The EDX mapping images of C, Fe, Cl and the overlay of C, Fe, Cl signals are shown in Figure 2e-2i. The obtained images show uniform distributions of C, Fe and Cl across the whole graphite region, indicate that $FeCl_2$ nanocrystals disperse uniformly in the graphite sheets. Notably, the intercalated $FeCl_2$ nanocrystals can hardly be washed off by ethanol due to the protection of impermeable graphite layers.

X-ray photoelectron spectroscopy (XPS) and Raman spectrum were taken to confirm the presence of Cl-doping on the graphite layers. **Figure 3**a shows the XPS scans of the top layers of the C-Cl/$FeCl_2$/C-Cl, which include C1s, Fe 2p, Cl 2p, Cl 2s and O1s. As shown of the Cl 2p XPS signals in Figure 3b, there are three spin–orbit doublets corresponding to Cl atoms in different chemical state. The presence of Cl $2p_{3/2}$ and Cl $2p_{1/2}$ XPS signals at 199.2 and 200.8 eV can be attributed to the chlorine in $FeCl_2$.[23] The peaks located at 200.4 eV ($2p_{3/2}$) and 201.7 eV ($2p_{1/2}$) can be attributed to C-Cl.[19,20,24] The prominent Cl 2p peaks at 198.3 eV ($2p_{3/2}$) and 199.8 eV ($2p_{1/2}$) can to be attributed to chlorine intercalated between the graphite layers.[23] In Figure 3c, the peaks at 284.8 eV of the pristine EG correspond to C 1s of sp^2 hybridized carbon. While, the lowering of the binding energy of the C 1s peak for the C-Cl/$FeCl_2$/C-Cl might be due to the lowering of the Fermi level caused by the chlorine dopant which introduces by charge transfer from the graphite layer planes.[25-27] Fe $2p_{3/2}$ core level peaks of the C-Cl/$FeCl_2$/C-Cl are shown in Figure S3, which are characteristic of Fe^{2+} in $FeCl_2$.[28]

Figure 3d shows the typical Raman spectra recorded for EG and the C-Cl/$FeCl_2$/C-Cl. Compared to EG, the peak at around 673 cm^{-1} immerged in the as-prepared sample corresponding to a C-Cl vibration, further confirmed the presence of chlorine atoms bound to the graphite substrate.[29] The G band is attributed to the C-C bond vibration, while the origin of the D band derived from structural disorders caused by changes in the hybridization of carbon from sp^2 to sp^3.[19] The Cl-doped samples show apparently higher ID/IG (0.168) than the pristine EG, indicating a reduction in the average size of the sp^2 domains after doping. Notably, the Raman G peak experienced a blue shift from 1581.2 cm^{-1} to 1582.9 cm^{-1}, indicating a hole doping effect during the chlorination treatment.[17,19] Besides, Raman spectra of the intermediate product (with annealing time of 12 h) were recorded. Compared to the intermediate product, the D band of the C-Cl/$FeCl_2$/C-Cl shows a Raman peak shift towards high frequency and intensity reduction. This interesting phenomenon provides further evidence of the π-electrons transfer from the graphite layer to chlorine,[30] which is in coincidence with the XPS results.

To evaluate the electrochemical properties of the as-prepared C-Cl/$FeCl_2$/C-Cl for LIBs application, galvanostatic discharge–charge, cyclic voltammetry (CV) and cycling measurements were conducted at room temperature in the voltage window of 0.01-3.0 V. **Figure 4**a presents the first three cycle's voltage versus capacity profiles of the C-Cl/$FeCl_2$/C-Cl at a current density of 200 mA g^{-1}. The first discharge and charge capacities are 1009 mA h g^{-1} and 647.7 mA h g^{-1} for the sample, indicating an irreversible loss of about 35.8%. This initial irreversible loss could be due to the decomposition of electrolytes to form a SEI layer on the surface and partial irreversible decomposition of LiCl during the first charge process, similar to that in previously reported $FeCl_3$-Graphite Intercalation Compounds anodes.[22,31] The following discharge/charge profiles of the sample shows two distinct potential regions above and below 0.3 V, which is consistent with that obtained from CV measurements (Figure S4). The potential below 0.3 V with pair of reduction/oxidation peaks from CV (Figure S4) shows a capacity of 236.7 mAh g^{-1}, corresponding to the conventional lithium intercalation/deintercalation processes in the natural interlayer of graphite (Li-GICs). The curve shape above 0.3 V has a capacity of 411 mAh g^{-1}. The capacity most likely derived from the formation of LiCl accompanying the emergence of Fe nanoparticles in the graphite layers ($FeCl_2 + 2\ Li^+ + 2e^- \rightarrow Fe + 2LiCl$), as the cathodic peaks shown in potential regions (above 0.3 V) from CV. Ex situ HRTEM image of the electrode (Figure 4b) after initial discharged to 0.01 V, confirmed the presence of Fe nanoparticles (3-6 nm) evenly distributed in the graphite layers (see Figure S5 for STEM image). Notably, the capacity (411 mAh g^{-1}) is much larger than the estimated capacity of 145 mAh g^{-1} from the content of $FeCl_2$ (Figure S6). The excess capacity is probably comes from the p-type Cl-doping induced π-electrons transfer from the graphite layer to chlorine. The π-electron delocalization may induce "activation region" on the surface of graphite layers and consequently improve the reversible capacity of the electrode (see supporting information Figure S7). Such phenomenon is common in other p-type doped electrode materials. For example, it has been demonstrated that the presence of BC_3 nanodomains in B-doped graphene and the pyridinic N atoms in N-doped graphene were able to improve the reversible capacity of the doped graphene electrode.[12-16]

The cycling performance of the sample and EG were evaluated at 500 mA g^{-1} in the voltage range of 0.01–3 V. As shown in Figure 4c, the reversible capacities of the C-Cl/$FeCl_2$/C-Cl slightly decrease in the initial three cycles and then increase with cycling and reach 1043 mA h g^{-1} after 350 cycles, which is approximately 28 times higher than that of the EG electrode (37.2 mAh g^{-1}). The coulombic efficiency is about 99% (Figure S8). The increase in capacity with cycling probably attribute to the activating process of the graphite with defect and the reversible formation/dissolution of polymeric gel-like film resulted from electrolyte degradation similar to that of transition metal oxides.[32] In addition, the long turn cycling performance of the C-Cl/$FeCl_2$/C-Cl was evaluated at current rate of 1000 mA g^{-1} (Figure 4d). It delivers a capacity of 516 mA h g^{-1} with 100% capacity retention over the test period of 1000 cycles, and the coulombic efficiency is almost 99%. The result further testifies extraordinary cycling stability of the composite electrode even at high charge/discharge rates. Besides the high capacity and good cycling stability, the rate performance is also an important characteristic for high performance LIBs (Figure 4e). As the current densities increase from 0.2, 0.5, 1, 2, 3, 5, 7 to 10 A g^{-1}, the C-Cl/$FeCl_2$/C-Cl exhibits excellent capacity retention, slightly varying from 615, 501, 408, 334, 298, 251, 211 to 161 mAh g^{-1},

which are much better than those of the EG. When the current rate turns back to 0.2 A g^{-1}, the capacity can be retained as high as 1286 mA h g^{-1} even after 200 cycles (Figure S9), suggesting the good rate capacity and structure stability of the active material.

The outstanding electrochemical performance of the C-Cl/$FeCl_2$/C-Cl comes from the combination of the advantages in its sandwich structure and p-type Cl-doping of graphite layers. Firstly, owing to the unique combination, a higher reversible capacity can be obtained. The sandwich structure enables three mechanisms of lithiation reaction: Li-ion intercalation/deintercalation in the graphite interlayers; Li-ion adsorption/desorption on the surface of the graphite sheets; and the formation/decomposition of LiCl from the electrochemically active species $FeCl_2$ nanocrystals, thus resulting in a larger capacity than pure graphite. Also, Cl-doping induced π-electron delocalization may produce "activation region" on the surface of graphite layers, enable the doped graphite to be favorable for Li storage and consequently improve the reversible capacity of the electrode. Secondly, the sandwich stacked structure provides an elastic buffer space to accommodate the volume changes of $FeCl_2$ nanocrystals during lithium-ion insertion/extraction, and, therefore, a better cycle performance can be obtained. Thirdly, the sandwich structure and Cl doping will improve the electrical conductivity and ionic conductivity of the composites and thus lead to an excellent high-rate electrochemical performance. It is reported that, sandwich structure can possess the shorter electronic transport length (*L*e), the fast and versatile transport pathways for the electrolyte ions and the continuous conductive path between nanocrystals.[4,5] And Cl-doping could enhance the electric conductivity of the carbon materials due to a p-type doping effect resulting from the presence of electronegative Cl atoms.[17,18] The electronic conductivity of C-Cl/$FeCl_2$/C-Cl measured by a four-probe method is 109.91 S cm^{-1} at room temperature, which is higher than that of EG (80.17 S cm^{-1}). The superior ionic conductivity of C-Cl/$FeCl_2$/C-Cl was confirmed by the clearly reduced diameter of the semicircle at the high-frequency region in the electrochemical impedance spectroscopy (EIS) patterns (Figure S10). All the above characteristics make the composite favorable for the storage of Lithium ions and consequently result in superior rate capability, high capacity, and cycle performance during the rapid charge-discharge process.

In conclusion, we have successfully employed a space-confined nanoreactor strategy to synthesize $FeCl_2$-graphite sandwich composite with Cl doping in graphite layers. Our sandwich structure has effectively inhibited the instability of $FeCl_2$ nanocrystals in environment. When evaluated as the anode material for rechargeable Li-ion batteries, the C-Cl/$FeCl_2$/C-Cl delivered a reversible capacity as large as 1043 mAh g^{-1} at a current density of 500 mA g^{-1} after 350 cycles, and exhibits almost 100% capacity retention after 1000 cycles at 1000 mA g^{-1}. We attribute the outstanding electrochemical performance to the combinative merits of $FeCl_2$ nanocrystals, sandwiched structures and Cl-doping of graphite layers, which provides excellent electrical conductivity and ionic conductivity, higher reversible capacity derived from the sandwich composite and π-electron delocalization of graphite layers, and enough elastomeric space to accommodate volume changes of $FeCl_2$ nanocrystals upon Li insertion/extraction. The design of such sandwich structure may enable new possibilities for the application of the instable materials. Furthermore, together with the novel Cl-doping of carbon, this sandwich-like composite may give a thread for exploring new types of anode materials for LIBs and other batteries using carbon as electrode.

Acknowledgements

This work was supported by the 973 Project of China (no. 2011CB935901), and the National Natural Science Fund of China (no. 91022033, 21201158).

Notes and references

Hefei National Laboratory for Physical Science at Microscale and Department of Chemistry, University of Science and Technology of China, Hefei, Anhui 230026, PR China. Fax: 86-551-63607402; Tel: 86-551-63602942; E-mail: ytqian@ustc.edu.cn(Y. Qian), ychzhu@ustc.edu.cn (Y. Zhu)

† Electronic Supplementary Information (ESI) available: [Experimental section and Figure S1-S8]. See DOI: 10.1039/b000000x/

1 M. Arm and J. M. Tarascon, *Nature*, 2008, **451**, 652.
2 N. A. Kaskhedikar and J. Maier, *Adv. Mater.*, 2009, **21**, 2664.
3 S. Yang, X. Feng and K. Müllen, *Adv. Mater.*, 2011, **23**, 3575.
4 X. Wang, X. Cao, L. Bourgeois, H. Guan, S. Chen, Y. Zhong, D. M. Tang, H. Li, T. Zhai and L. Li, *Adv. Funct. Mater.*, 2012, **22**, 2682.
5 X. Wang, W. Tian, D. Liu, C. Zhi, Y. Bando and D. Golberg, *Nano Energy*, 2013, **2**, 257.
6 L. Ji, Z. Tan, T. Kuykendall, E. J. An, Y. Fu, V. Battaglia and Y. Zhang, *Energ. Environ. Sci.*, 2011, **4**, 3611.
7 N. Li, G. Zhou, R. Fang, F. Li and H. M. Cheng, *Nanoscale*, 2013, **5**, 7780.
8 J. Xie, X. Sun, N. Zhang, K. Xu, M. Zhou and Y. Xie, *Nano Energy*, 2013, **2**, 65.
9 W. Zhang, W. Wan, H. Zhou, J. Chen, X. Wang and X. Zhang, *J. Power Sources*, 2013, **223**, 119.
10 S. Yang, X. Feng, L. Wang, K. Tang, J. Maier and K. Müllen, *Angew. Chem. Int. Edit.*, 2010, **49**, 4795.
11 C. Zhang, N. Mahmood, H. Yin, F. Liu and Y. Hou, *Adv. Mater.* 2013, **25**, 4932.
12 Z. S. Wu, W. Ren, L. Xu, F. Li and H. M. Cheng, *Acs Nano*, 2011, **5**, 5463.
13 I. Mukhopadhyay, N. Hoshino, S. Kawasaki, F. Okino, W. K. Hsu and H. Touhara, *J. Electrochem. Soc.*, 2002, **149**, 39.
14 Y. Li, Z. Zhou and L. Wang, *J. Chem. Phys.*, 2008, **129**, 104703.
15 L. Bulusheva, A. Okotrub, A. Kurenya, H. Zhang, H. Zhang, X. Chen and H. Song, *Carbon*, 2011, **49**, 4013.
16 A. L. M. Reddy, A. Srivastava, S. R. Gowda, H. Gullapalli, M. Dubey, and P. M. Ajayan, *Acs Nano*, 2010, **4**, 6337.
17 X. Zhang, A. Hsu, H. Wang, Y. Song, J. Kong, M. S. Dresselhaus and T. Palacios, *ACS nano*, 2013, **7**, 7262.
18 J. Y. Kim, W. H. Lee, J. W. Suk, J. R. Potts, H. Chou, I. N. Kholmanov, R. D. Piner, J. Lee, D. Akinwande and R. S. Ruoff, *Adv. Mater.*, 2013, **25**, 2308.
19 B. Li, L. Zhou, D. Wu, H. Peng, K. Yan, Y. Zhou and Z. Liu, *ACS nano*, 2011, **5**, 5957.
20 L. Oliveira, F. Lu, L. Andrews, G. A. Takacs, M. Mehan and T. Debies, *J. Mater.* Res. **2014**, *29*, 239.
21 H. Sahin and S. Ciraci, *J. Phys. Chem. C*, 2012, **116**, 24075.
22 L. Wang, Y. Zhu, C. Guo, X. Zhu, J. Liang and Y. Qian, *ChemSusChem*, 2014, **7**, 87.
23 N. A. Vinogradov, K. Simonov, A. Generalov, A. Vinogradov, D. Vyalikh, C. Laubschat, N. Mårtensson and A. Preobrajenski, *J. Phys-Condens. Ma.*, 2012, **24**, 314202.

24 J. Zheng, H. T. Liu, B. Wu, C. A. Di, Y. L. Guo, T. Wu, G. Yu, Y. Q. Liu and D. B. Zhu, *Sci. Rep.*, 2012, **2**, 662.
25 U. Dettlaff-Weglikowska, V. Skákalová, R. Graupner, S. H. Jhang, B. H. Kim, H. J. Lee, L. Ley, Y. W. Park, S. Berber and D. Tománek, *J. Am. Chem. Soc.*, 2005, **127**, 5125.
26 H. J. Shin, S. M. Kim, S. M. Yoon, A. Benayad, K. K. Kim, S. J. Kim, H. K. Park, J. Y. Choi and Y. H. Lee, *J. Am. Chem. Soc.*, 2008, **130**, 2062.
27 T. Shirasaki, A. Derré, M. Ménétrier, A. Tressaud and S. Flandrois, *Carbon*, 2000, **38**, 1461.
28 A. P. Grosvenor, B. A. Kobe1, M. C. Biesinger and N. S. McIntyre, *Surf. Interface Anal.*, 2004, **36**, 1564.
29 A. M. Debela, M. Ortiz, V. Beni and C. K. O'Sullivan, *Chem. Eur. J.*, DOI: 10.1002/chem.201402051.
30 H. Zhu, C. Xiao, H. Cheng, F. Grote, X. Zhang, T. Yao, Z. Li, C. Wang, S. Wei, Y. Lei and Y. Xie, *Nat. Commun.*, 2014, **5**.
31 F. Wang, J. Yi, Y. Wang, C. Wang, J. Wang and Y. Xia, *Adv. Energy Mater.* 2014, **4**.
32 S. Grugeon, S. Laruelle, L. Dupont and J. M. Tarascon, *Solid State Sci.* 2003, **5**, 895.

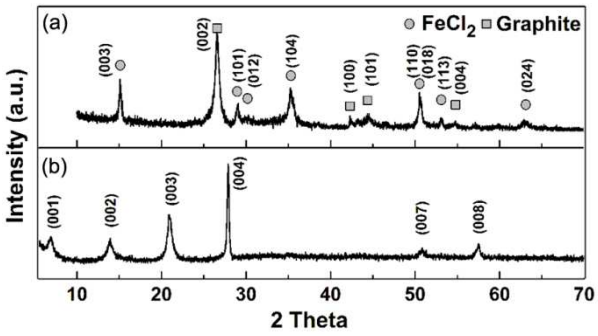

Figure 1. XRD patterns of (a) the C-Cl/$FeCl_2$/C-Cl and (b) the stage 2 $FeCl_3$-GICs.

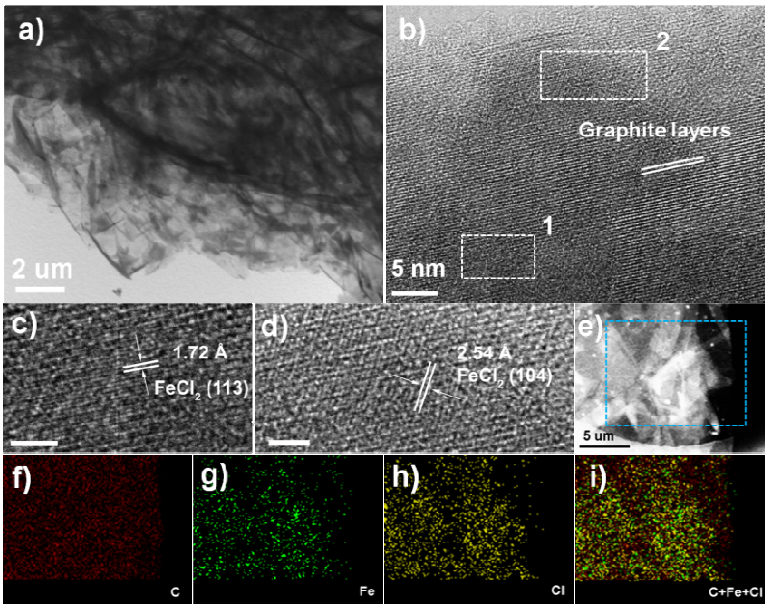

Figure 2. Characterization of C-Cl/$FeCl_2$/C-Cl: (a) TEM image; (b) HRTEM image; (c) and (d) Magnified HRTEM image of the lattice fringe as highlighted by dotted box 1and 2 in (b), respectively; (e) scanning transmission electron microscopy (STEM) images, (f-i) the corresponding EDX elemental mapping of C, Fe, Cl and along with an overlay of those three maps in the selected area (blue rectangle in (e)).

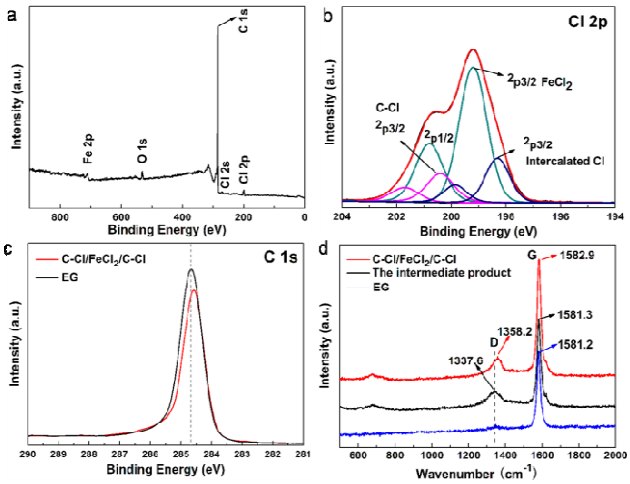

Figure 3. (a) XPS survey spectra of the C-Cl/$FeCl_2$/C-Cl (b) XPS Cl 2p spectrum, (c) XPS C1s spectrum for the C-Cl/$FeCl_2$/C-Cl and EG; (d) Raman spectrum of the samples.

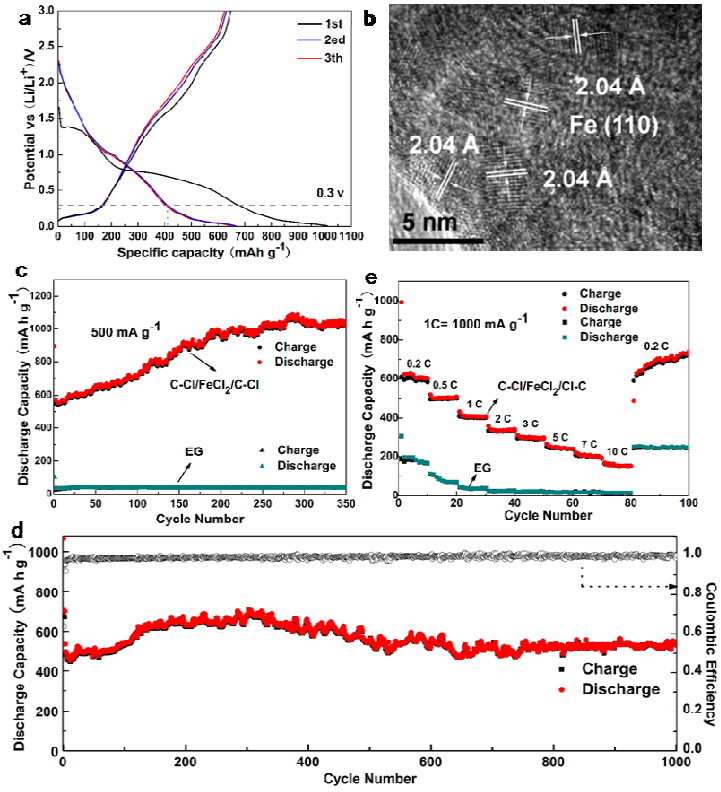

Figure 4. (a) Charge and discharge profiles of the C-Cl/$FeCl_2$/C-Cl at 0.2 A g^{-1} for the first three cycles. (b) Ex situ HRTEM image of the C-Cl/$FeCl_2$/C-Cl electrode after full discharge. (c) Cycle performances of the C-Cl/$FeCl_2$/C-Cl and EG at a current density of 500 mA g^{-1}. (d) Cycle performance of C-Cl/$FeCl_2$/C-Cl at a current of 1000 mA g^{-1}. The first three cycles are conducted at a current density of 100 mA g^{-1} to activate the electrode materials; (e) Rate performance. The sign "C" represent a current density of 1000 mA g^{-1}.